Landfast ice in the Kara Sea stabilizes the Arctic halocline and may slow down Atlantification of the Eurasian Basin

Yuqing Liu[1*], Martin Losch[1*], Bruno Tremblay[2] and Markus Janout[1]

[1*]Alfred-Wegener-Institut, Helmholtz-Zentrum für Polar-und Meeresforschung, 27570, Bremerhaven, Germany.
[2]Department of Atmospheric and Oceanic Sciences, McGill University, H3A 0B9,Montreal, Quebec, Canada .

*Corresponding author(s). E-mail(s): Yuqing.Liu@awi.de; Martin.Losch@awi.de;
Contributing authors: Bruno.Tremblay@mcgill.ca; Markus.Janout@awi.de;

Abstract

Observations show an Atlantification of the Eurasian Basin of the Arctic Ocean, with deeper penetration, shoaling, and ventilation of Atlantic waters in the eastern Arctic and an associated weakening of the cold halocline layer. These processes have a profound impact on the sea ice cover above and potentially on the transition of the Arctic to a seasonal ice cover. Here we show, using a coupled ice-ocean model, that a proper simulation of the landfast ice cover in the relatively small but deeper peripheral Kara Sea has a disproportionately large influence on the halocline stability in the Eurasian Basin and beyond. Specifically, landfast ice in the Kara Sea reduces ice growth and therefore salt rejection into the surface ocean. This negative salinity anomaly is advected eastward with a coastal current along the continental shelf in the Makarov Basin and then out of the Arctic through Fram Strait by the Transpolar Drift Stream on timescales of less than ten years. Global Climate Models, however, do not yet include landfast ice parameterizations. Therefore, they are missing this key process affecting the halocline stability, Atlantification of the Makarov Basin, and potentially the timing of a seasonally ice-free Arctic.

Keywords: Landfast ice, Arctic hydrography, Lateral drag parameterization

1 Introduction

Landfast ice (LFI) – sea ice that stays fast along the coast where it is attached to the shore or over shoals [1] – can extend a few kilometers (e.g., Beaufort Sea, Western Laptev Sea) to several hundred kilometers into the ocean (e.g., Kara Sea, East Siberian Sea, Eastern Laptev Sea). Its presence is associated with specific bathymetry and coastline features. For instance, it can be grounded on the ocean floor by pressure ridges in shallow water and over shoals (Stamukhi) [2–7]; it can be attached to coastlines by local tensile forces or compressive forces from distant land protrusion along the coast [8]; or it can be supported by offshore islands [9]. LFI plays an important role in polar coastal regions. It decreases the energy, momentum, and heat flux between the atmosphere and the ocean, and thereby reduces surface ocean mixing [4, 10–12]. This extension of the land also provides a platform for hunting, tourism, scientific research, oil and gas exploration, and serves as a habitat for polar wildlife [13–16].

At the seaward end of LFI, flaw-lead polynyas [5] form as openings between stationary fast ice and mobile pack ice. In these flaw polynyas, large air-sea heat fluxes, sea ice growth, and associated salt rejection lead to the formation of dense waters. These cold dense waters spill over the continental shelves and find their level of neutral buoyancy between the warm salty Atlantic and the cold fresher surface water, where they form the cold halocline layer [17, 18]. This cold halocline layer acts as a buffer between the two water masses and leads to significant sea ice growth in winter and the formation of a perennial sea ice cover: when ice growth and salt rejection drive surface convection, cold and saltier surface water sinks to the base of the mixed layer.

There, it is still well above the warm water, and brings (still) cold halocline water at the freezing point into the mixed layer. This process does not lead to vertical transport of ocean heat because it does not reach the warm water, in contrast with the Southern Ocean where the thermocline coincides with the halocline [19].

The recent Atlantification of the Eurasian Basin, that is, the eastward progression of warmer Atlantic Water into the eastern Arctic, has led to shoaling of the intermediate-depth Atlantic Water layer and a weakening of the halocline, increasing ocean-interior ventilation in winter [20–22]. Subsequently, the associated enhanced release of oceanic heat reduced winter sea ice formation in the Eurasian Basin [23]. Should the cold halocline disappear, the Atlantification of the Arctic would ventilate significant Atlantic water heat in winter leading to a seasonal sea ice cover in the Eurasian Basin [24]. A retreat of the cold halocline, as documented in the early 1990's [25], can affect the shelf hydrography and the formation of the cold halocline waters in the Makarov Basin [26].

This work presents evidence for a significant impact of an LFI cover in the Kara Sea —— a feature that is missing in current Earth System Models because of the absence of fast ice parameterizations —— on the local salt budget. Without LFI, local ice formation modifies the fresh surface water provided by the large river systems to a local coastal current so that too salty water leaves the Kara Sea. This salinity anomaly signal increases the stability of the halocline over the entire Eurasian Basin.

2 Results

2.1 More landfast ice in the Kara Sea, fresher surface water in the interior Arctic

We activate different parameterizations of LFI that result in the presence or absence of LFI in specific parts of the model domain (see Methods section 5). More LFI makes the shelves fresher [17], but more LFI in the Kara Sea also makes the halocline in the interior Arctic (approximately the top 40 m) fresher (Figure 1). This negative salinity anomaly in the interior Arctic Ocean reduces the salinity bias of our model relative to observations. As observational reference, we use an average of 20 salinity casts from the Unified Database for Arctic and Subarctic Hydrography (UDASH) [27, 28] that were collected in all Aprils of our simulation period of 2006–2015 in the region between 120°–180°E and north of 75°N (approximately the Makarov Basin). Compared to this average, the control simulation (CTRL) is too saline by 0.88. This mean difference reduces to 0.58 for the simulation with LFI. The root-mean-square difference also reduces from 1.27 to 1.06.

The simulation with the fast ice parameterization (Figure 1b) produces higher ice concentration (less open water available for sea ice formation) along the coastlines in the Beaufort, East Siberian, Laptev, and Kara Seas, and lower ice concentration (more open water available for more sea ice formation in flaw polynyas) offshore. This is consistent with previous results [17]. The formation of sea ice generally leads to a local increase of surface salinity as most of the salt of seawater is left behind and not included in new sea ice. A stable LFI cover inhibits new ice formation where the continuous export of ice in the control simulation leads to continuous new ice formation and increase of salinity. Therefore, the surface water is fresher (less saline) underneath the stable LFI cover of the simulations with fast ice parameterization compared to the control simulation (Figure 1b). This is particularly evident in the Laptev and East Siberian seas (Figure 1b). Northward of the LFI edge in the East Siberian Sea, the upper ocean is more saline than in the control simulation, again in accord with previous results [17]. Offshore winds in the East Siberian Sea drive ice northwards and form polynyas at the edge of the LFI where new ice formation leaves more salt behind and increases the local surface salinity.

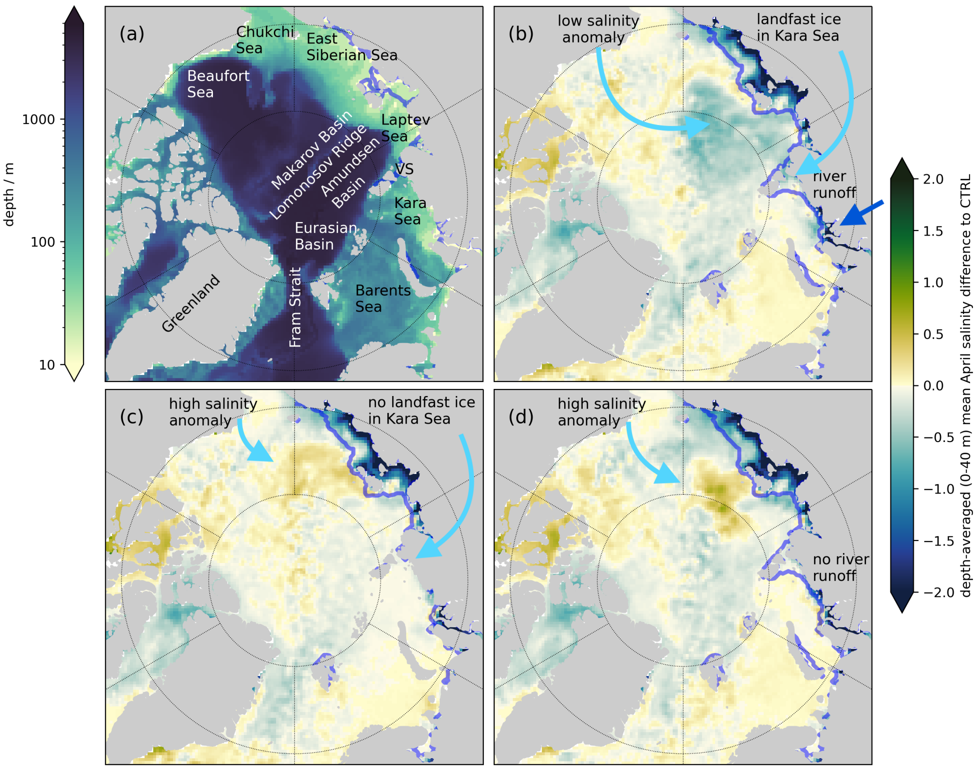

Fig. 1 (a) Arctic topography. VS denotes the Vilkitsky Strait. The blue contour line denotes the (poorly) simulated fast ice extent in the control run (CTRL, without fast ice parameterization). (b)–(d) Depth averaged (0–40 m) salinity differences for the mean April of 2006–2015: (b) between the simulation with all fast ice parameterizations, i.e., with a realistic LFI distribution as indicated by the blue contour line, and CTRL simulation; (c) the same as (b), but with the lateral drag parameterization turned off explicitly in the Kara Sea; there is no LFI in the Kara Sea as indicated by the blue contour line; (d) the same as (b), but without river runoff in the Kara Sea and in CTRL; there is slightly less LFI in the Kara Sea as indicated by the blue contour line.

In the Kara Sea, an additional LFI parameterization [8] also leads to an LFI cover where the water is deeper and ice keels alone fail to stabilize the LFI cover (Figure 1b). In contrast to the local effects in and near the shallow East Siberian and Laptev Seas, LFI in the relatively deep Kara Sea leads to a much fresher upper ocean that spreads with a well-known coastal current that also carries river water along the Taymyr Peninsula and through the Vilkitsky Strait (between the Laptev and Kara Seas, Figure 1b) into the Makarov Basin [29, 30]. We emphasize that this low salinity anomaly in the Makarov Basin is almost entirely caused by the additional LFI in the

Kara Sea. In a simulation where the new LFI parameterization [8] is turned off, there is no LFI in the Kara Sea and the fresh anomaly in the Makarov Basin disappears (Figure 1c).

As a further piece of evidence for the suggested mechanism, the amplitude of the negative salinity anomaly in the Kara Sea and the Makarov Basin decreases in an experiment where the river runoff in the Kara Sea is turned off (in both control and sensitivity experiments). Instead, a positive anomaly appears north of the New Siberian Islands (Figure 1d). From this, we conclude that the river runoff provides a large contribution to transporting the low salinity signal in the upper ocean from the Kara Sea to the Makarov Basin (Figure 2).

Previous results suggest that the path of the Ob and Yenisei river water [29, 30] coincides with the spreading of the low salinity water leading to the anomaly in Figure 1b. To show that this is the case in our model, we trace the river runoff from the Ob and Yenisei Rivers in the Kara Sea with a passive tracer (Figure 2). The passive tracer exits the Kara Sea through the Vilkitsky Strait. A portion enters the Laptev Sea while the remainder subducts into the Amundsen and Makarov Basins. The tracers are then advected by the Transpolar Drift Stream over the Lomonosov Ridge and finally exit through Fram Strait (Figure 2). The distribution of passive tracer of the Ob and Yenisei water resembles observed patterns based on chemical tracer-based water mass analyses [29, their Figure 3b]. The tracer pattern is also very similar to the pattern of the low salinity signal in the upper ocean (Fig. 1), implying a freshwater transport path from the Kara Sea to the Makarov Basin.

A Hovmöller diagram along the dashed line in Figure 2a of the depth-averaged (0–40 m) salinity and salinity difference between different experiments illustrates the transport of the low salinity signal from the Kara Sea to the Chukchi Sea (Figure 3). The difference between simulations with and without LFI in the Kara Sea clearly shows that salinity anomalies in the Makarov Basin originate from the Kara Sea, and

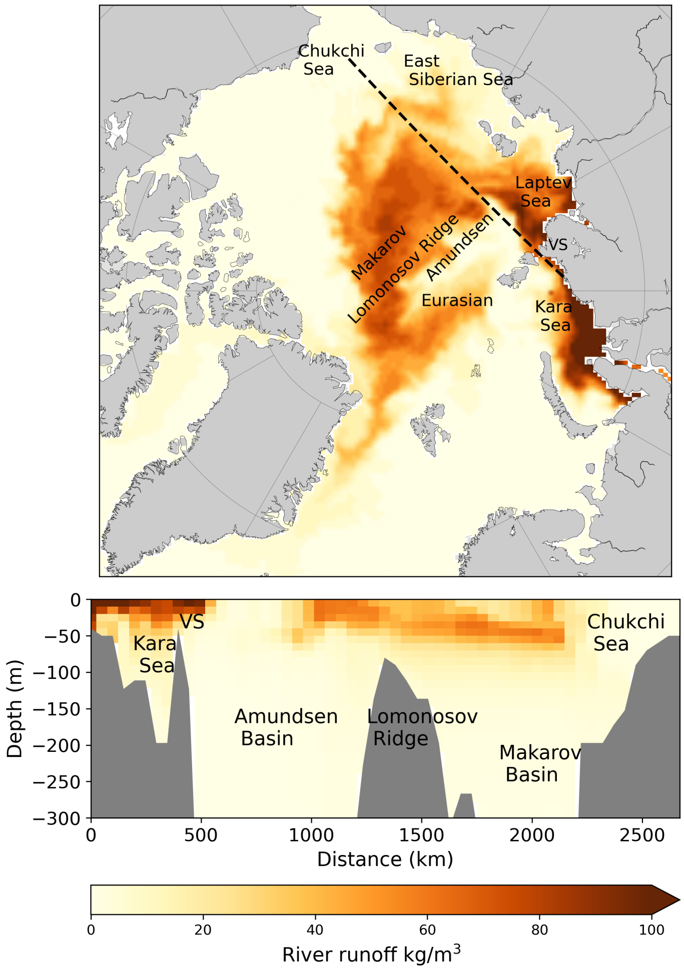

Fig. 2 (a) Depth averaged (0–40 m) passive tracer of the river runoff from the Kara Sea in April 2015 in the control run. (b) Vertical distribution of the passive tracer along a section marked by the dashed line in panel (a) starting from the Kara Sea into the Chukchi Sea.

that local salinity anomalies in the Laptev or East Siberian seas are not responsible for the negative salinity anomaly in the Makarov Basin.

Very early in the simulation without LFI in the Kara Sea, a positive salinity anomaly develops locally at the edge of the polynya in the Laptev and East Siberian seas (1500–2200 km, after 2001 during the spinup, Figure 3c), because new ice formation releases salt into the ocean. This anomaly persists until the end of the simulation (see also light blue arrow in Figure 1c). The same positive salinity anomaly in

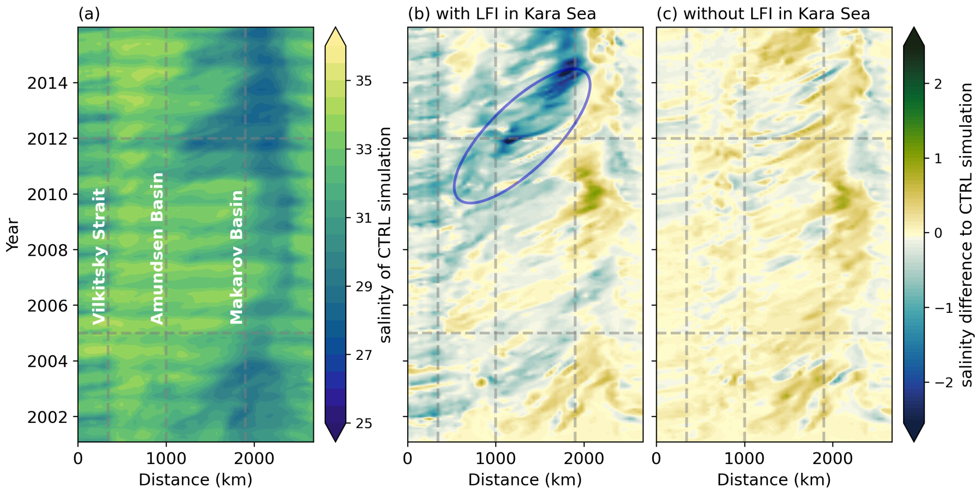

Fig. 3 Hovmöller diagram along the dashed line in Figure 2a for years 2001 to 2015 (2001–2005 is a spin-up) of depth-averaged (0–40m) (a) salinity in the control simulation (CTRL); (b) salinity difference between the simulation with LFI in the Kara Sea) and the control simulation (corresponding to Figure 1b); (c) salinity difference between the simulation without LFI in the Kara Sea and the control simulation (corresponding to Figure 1c). The blue ellipse marks the strong negative salinity anomaly described in the text. The x-axis is the distance in kilometers along the transect (dashed line) in Figure 2a. The dashed vertical lines parallel to the y-axis indicate the approximate locations of the Vilkitsky Strait, the Amundsen and the Makarov Basins (from left to right), and the lower dashed horizontal lines mark the end of the spin-up and the upper ones the beginning of the large positive salinity anomaly in 2012.

the Makarov Basin also appears early in the simulation with LFI in the Kara Sea (Figure 3b). But here, and in contrast to the locally generated signal, low salinity of the Kara Sea is advected to the Makarov and Eurasian Basins as early as 2002. There are smaller pulses of negative salinity anomaly moving from the Kara Sea to the Makarov Basin throughout 2001–2007. This process increases in 2008, with a negative salinity anomaly peak in 2012 (blue ellipse in Figure 3b).

2.2 Salt budget analysis

The salt content in the Arctic Ocean is determined by surface forcing, advection, and to a very small extent by diffusion between the surface and deeper ocean layer (see Methods section 5). The differences in salt content, salt advection and diffusion between the simulation with and without LFI parameterization in the Kara Sea are

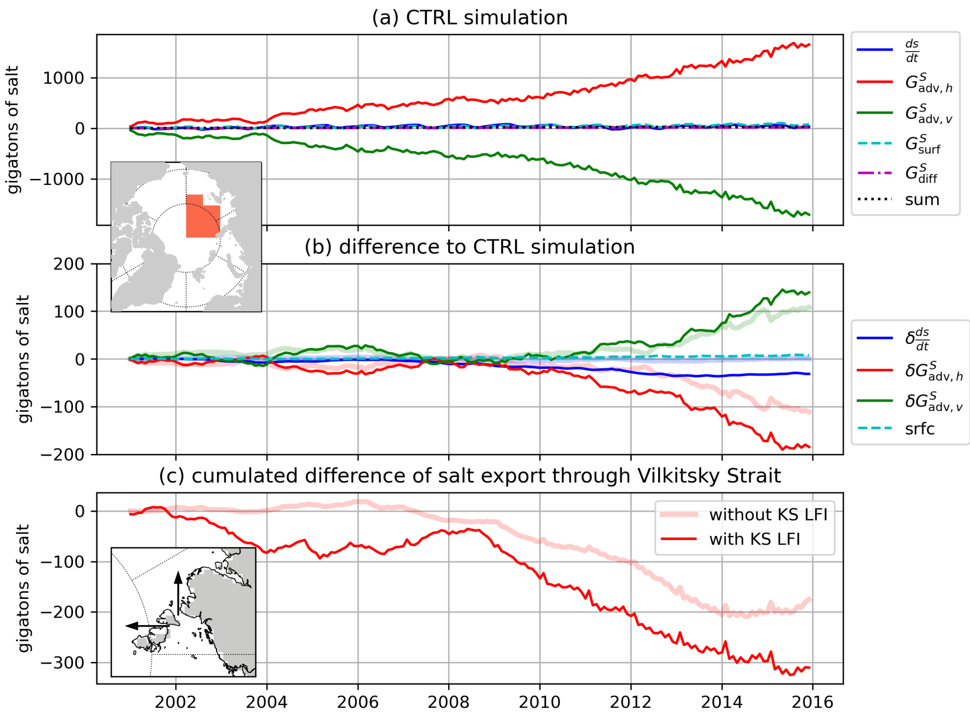

Fig. 4 Time series of (a) accumulated salt budget terms ($\int_0^t G(t')\,dt'$, see Eq. 1 in the Methods section) for the top four layers (40 m) of the Eurasian and Makarov Basin (see red area in the inset) for the CTRL simulation. The horizontal advection of salt ($G^S_{\mathrm{adv,h}}$, red lines) is balanced by vertical advection ($G^S_{\mathrm{adv,v}}$). (b) difference of simulations without and with LFI in the Kara Sea. With LFI (but not in the Kara Sea) the horizontal advection of salt is reduced, balanced by a reduction of downward advection (faint thick lines). With LFI also in the Kara Sea the downward advection decreases less than the horizontal advection, potentially because of increased stability, so that these terms no longer balance and the net salt content reduces (thin lines). (c) difference of accumulated salt flux relative to CTRL through the Vilkitsky Strait (in gigatons of salt, negative values mean a reduced salt flux). The flux is the combination of the flux through the actual Vilkitsky Strait and a small northward opening (see inset); red thin line: with LFI in the Kara Sea (KS); faint thick line: without LFI in the Kara Sea.

small when integrated over the entire model domain ($O(< 1\%)$ of the signal, results not shown). In the upper 40 m of the Makarov Basin, which we chose to approximate the halocline depth in our model, the mean salt content changes very little over time in the CTRL simulation. In the cumulative budget, however, the considerable horizontal advection of salt is balanced by downward vertical advection out of the 40 m surface layer (i.e. the halocline). Vertical diffusion and surface fluxes are small (Figure 4a).

In the simulation without LFI only in the Kara Sea, but with the additional LFI in other marginal seas (Figure 1c) and with less sea ice formation and salt release into the ocean, less salt is advected into the Makarov Basin, especially after 2012. This decrease of horizontal advection is balanced by reduced downward vertical advection of salt, leaving the mean salt practically unchanged (Figure 4b, thick lines). The reduction of salt advected into the Makarov Basin is even larger with LFI present in the Kara Sea (after 2008 and 2012). In this case, however, it is not balanced entirely by a reduction in downward vertical advection, probably because of the surface stratification and the mean salinity increase (Figure 4b, thin lines). The local reduction in horizontal advection between 2004 and 2008 is offset by vertical advection in this simulation supporting the notion that the magnitude of the horizontal advection anomaly is important in this balance and can lead to non-linear effects.

The salt leaves the Kara Sea mainly through the Vilkitsky Strait (Figure 4c). In the simulation with LFI in the Kara Sea, approximately 100 gigatons of salt are not advected out of the Kara Sea through the Vilkitsky Strait (Figure 4c), in line with the deficit of advected salt in the Makarov Basin.

3 Discussion

Landfast ice (LFI) affects the position of offshore polynyas and hence the location where sea ice forms over open water [17]. The altered freshwater flux and associated salinity forcing changes the stability of the halocline, which can be demonstrated with numerical models with adequate parameterization of landfast ice [17]. A new parameterization that allows to selectively enable LFI in the Kara Sea [8] makes it possible to include its effects. The effect on the Makarov Basin hydrography is surprisingly large given the small size of the Kara Sea compared with other marginal seas (e.g., Laptev Sea, East Siberian Sea). The significant decrease in salinity within the top 40 meters of the water column (approximately the halocline in our model) in the Makarov Basin enhances the stability of the water column, while also correcting a saline model bias. Similarly, a reduction in LFI in the Kara Sea —– driven, for example, by climate change —– could decrease stability in the central Arctic Ocean, potentially accelerating Atlantification. This would allow warmer and more saline Atlantic waters to more easily reach the surface [31, 32], with profound implications for sea ice extent and seasonality.

More generally, the surface water in the Kara Sea, freshened by river water from rivers Ob and Yenisei, flows along the coast, through the Vilkitsky Strait, and into the Makarov Basin [29, 30]. Landfast ice along the coast causes polynyas to form off the fast ice edge and away from the core of the coastal current, so that salt rejection during sea ice formation does not modify the fresh surface water runoff. As a result, the waters exiting through the Vilkitski Strait are relatively fresh. In a model that does not reproduce landfast ice along the coast of the Kara Sea, the fresh surface water is modified by salt rejection in coastal polynyas that form in winter where the landfast ice should be, so that the water passing through the Vilkitsky Strait is too saline. This is most likely the situation for most numerical ocean and climate models as they underestimate the fast ice extent in the Kara Sea [3]. As a consequence, we speculate that current ocean and climate models underestimate the stability of the Arctic halocline and potentially overestimate Atlantification.

As landfast ice in the Kara Sea is supported by arching of the ice [33], models with non-zero tensile strength or larger maximum viscosities in the sea-ice rheology also simulate realistic landfast ice distributions in the Kara Sea [4, 33] with similar consequences for the halocline stability [18]. Here, we can cleanly separate the LFI effects from changes in sea ice cover due to the modified rheology [18], but in general, the results are robust with respect to the specific rheological modifications used to simulate landfast ice in the Kara Sea.

The negative surface salinity anomaly in our simulation with LFI in the Kara Sea travels from the Kara Sea to the Makarov Basin soon after the start of the model run, but there are two larger transport anomaly episodes (2002–2006 and 2008–2015) driven by specific wind-forcing anomalies [34, 35]. The negative salinity difference in the upper ocean is largest after the end of summer in 2012 (Figure 3b), presumably because of the large sea ice retreat in 2012. In August 2012, an intense storm increased mixing in the ocean boundary layer, increased upward ocean heat transport, and caused bottom melt that reduced the sea ice volume about twice as fast as in other years [36]. Eventually, the sea ice extent at the end of the summer in 2012 was smaller than it had been since the beginning of the satellite record in the late seventies [37]. These processes were also at play in our simulation and the mean simulated sea ice extent reached its lowest value of the simulation in 2012 (not shown).

The Kara Sea receives freshwater discharge from the Ob and Yenisei Rivers, which carry over one-third of the total freshwater discharge in the Arctic [30]. This water then travels with a coastal current, leaves the Kara Sea through the Vilkitsky Strait, and eventually reaches the Makarov Basin [29, 30]. In our simulation, a passive tracer for Ob and Yenisei water agrees with the observed Ob and Yenisei water distribution [29, 38] giving us faith in the accuracy of that aspect of our simulation. The simulated tracer distribution illustrates the path of the river runoff and hence any surface anomaly from the Kara Sea to the Makarov Basin via the Vilkitsky Strait (Figure 2). In our simulations, the LFI in the Kara Sea leads to a deficit of about 100 gigatons of salt leaving the Kara Sea by the end of the simulation (Figure 4c). This deficit in the horizontal advection is so large that it cannot be balanced by the vertical transport of salt in the Makarov Basin, because the vertical transport, mostly vertical advection, needs to overcome an increasing stability.

The Arctic mixed layer is important to physical, chemical, and biological processes. Simulating mixed layer dynamics accurately requires relatively high vertical resolution of the model grid. Our simulations are relatively coarse (10 m vertical grid spacing near the surface). Therefore, we do not expect that our simulation accurately represents the details of mixed layer dynamics. For example, we would need a dramatically refined vertical grid or even Large Eddy Simulations to study the impact of LFI on surface drivers for the change of the seasonal mixed layer depth, that is, sea ice thermodynamics (i.e., salt rejection during ice formation, freshwater input during ice melt) and wind-driven mixing [39] and their effect on the mixed layer depth. Further, we note that riverine heat, which is not considered in our model, is believed to be important in explaining the phenomena of freeze-up and sea ice melt along the Arctic coasts [40].

4 Conclusion

LFI in the Kara Sea changes the surface salinity of the central Arctic on timescales of a few years. In general, more LFI in the Arctic Ocean decreases the upper ocean salinity locally on the shelves in the Kara, Laptev, and East Siberian Seas. The largest effect, however, is found for the Kara Sea. Here, the relatively small LFI area induces a fresh anomaly in the upper ocean that is transported to the central Arctic Ocean. There, it leads to a surprisingly large salinity anomaly that increases the halocline stability. River runoff in the Kara Sea contributes to transporting the signal from the Kara Sea to the Makarov Basin. The negative salinity tendency observed with LFI on both shallow and deep shelves can be attributed mainly to reduced horizontal salt transport, which is not fully compensated by reduced vertical advective fluxes. These mechanisms become apparent after implementing a combination of a lateral and a basal drag parameterization in a pan-Arctic sea ice model to improve the simulation of LFI in the Arctic.

A sea ice model with a proper representation of LFI will improve our understanding of its influence on the hydrography in the Arctic. Our model simulations suggest that LFI in the Kara Sea stabilizes the water column in the central Arctic. Once the LFI in the Kara Sea disappears due to a warming Arctic, the stabilizing effect reduces within a few years and the Atlantification of the Arctic can accelerate.

5 Methods

We use a regional Arctic configuration of the Massachusetts Institute of Technology general circulation model (MITgcm) [41, 42] with a grid resolution of 36 km. This model resolves ocean and sea ice processes with a finite-volume discretization on an Arakawa C grid. The sea ice component includes zero-layer thermodynamics [43] and viscous-plastic dynamics with an elliptical yield curve and a normal flow rule [44, 45]. The model is forced by atmospheric fields from the global atmospheric reanalysis ERA-Interim data set [46]. The hydrography is initialized with temperature and salinity fields from the Polar Science Center Hydrographic Climatology 3.0 [47]. Details of the sea ice model can be found in [48, 49].

Without an explicit parameterization of LFI, sea ice models grossly underestimate the LFI extent. We implement two fast ice parameterizations: a basal drag parameterization [3] leads to realistic LFI areas in shallow marginal seas such as the Beaufort, Laptev and the East Siberian Seas, and a new fast ice parameterization where an explicit lateral drag that depends on the sub-grid-scale coastline length and orientation replaces the no-slip boundary condition of the sea ice momentum equations [8]. The latter parameterization leads to more LFI in the relatively deep Kara Sea, where the basal drag parameterization that relies on relatively shallow depths fails. Thus, the new parameterization can be used as a switch to turn on or off the LFI cover in the Kara Sea and other selected regions of the Arctic Ocean [8]. A control simulation (CTRL) without fast ice parameterization grossly underestimates LFI extent and timing. We make use of the fast ice parameterizations so that we can compare simulations with realistic LFI in all relevant regions and simulations where the parameterizations are turned off in selected regions such as the Kara Sea to the control simulation. For each configuration, the model is run from 2001 to 2015. The first five years constitute a spin-up during which the sea ice and surface ocean reach stable states for analysis.

Integrating the salt conservation equation leads to a salt budget equation. The change in salt content over time (G^S_{tot}) in a given volume V with total surface area A and interface area with the atmosphere A_{surf} is equal to the convergence of the advective (G^S_{adv}) and diffusive fluxes F_{diff} (G^S_{diff}), and a forcing term associated with surface salt flux F_{forc} (G^S_{forc}):

$$\underbrace{\frac{\partial s}{\partial t}}_{G^S_{\text{tot}}} = \underbrace{-\rho \oint_A uS\, da}_{G^S_{\text{adv}}} + \underbrace{\rho \iiint_V F_{\text{diff}}\, dx\, dy\, dz}_{G^S_{\text{diff}}} + \underbrace{\rho \iint_{A_{\text{surf}}} F_{\text{forc}}\, dx\, dy}_{G^S_{\text{forc}}}, \quad (1)$$

where $\mathbf{u}$ is the ocean velocity normal to the area, S is the salinity (in grams per kilograms of sea water), $s = \rho \iiint_V S\, dx\, dy\, dz$ is the salt content (in grams), $\rho = 1035\,\text{kg}\,\text{m}^{-3}$ is the sea water reference density, da is the area element. For our analysis we split the advective contribution into a horizontal $G^S_{\text{adv,h}}$ and a vertical part $G^S_{\text{adv,v}}$. Integrating Eq. 1 gives the accumulated salt contents $\int_0^t G(t')\, dt'$ for each term.

Acknowledgments

The authors thank Thomas Jung and Lars Kaleschke for constructive discussions.

Declarations

Funding: This work is supported by the DFG-funded International Research Training Group ArcTrain (IRTG 1904 ArcTrain).

Data availability: The salinity in the Unified Database for Arctic and Subarctic Hydrography (UDASH) is available from the PANGAEA data archive [27].

Code availability: The model data in this manuscript is based on the Massachusetts Institute of Technology general circulation model (MITgcm) [42], the version with lateral drag parameterization is available at https://doi.org/10.5281/zenodo.7954400 and the model configurations at https://doi.org/10.5281/zenodo.7919422.

Authors' contributions: YL and ML designed the experiments, YL carried them out and analyzed the data with help of ML, BT, and MJ. YL wrote the manuscript with contributions from ML, BT, and MJ.

References

[1] World Meteorological Organization. WMO sea-ice nomenclature. Terminology, codes and illustrated glossary. Tech. Rep., Secretariat of the World Meteorological Organization, Geneva (1970).

[2] Mahoney, A. R., Eicken, H., Gaylord, A. G. & Gens, R. Landfast sea ice extent in the Chukchi and Beaufort Seas: The annual cycle and decadal variability. *Cold Regions Science and Technology* **103**, 41–56 (2014).

[3] Lemieux, J. F. *et al.* A basal stress parameterization for modeling landfast ice. *Journal of Geophysical Research: Oceans* **120**, 3157–3173 (2015).

[4] Lemieux, J. F. *et al.* Improving the simulation of landfast ice by combining tensile strength and a parameterization for grounded ridges. *Journal of Geophysical Research: Oceans* **121**, 7354–7368 (2016).

[5] Rabault, J. *et al.* A dataset of direct observations of sea ice drift and waves in ice. *Scientific Data* **10**, 251 (2023).

[6] Kasper, J. L. & Weingartner, T. J. The spreading of a buoyant plume beneath a landfast ice cover. *Journal of Physical Oceanography* **45**, 478–494 (2015).

[7] Plante, M., Tremblay, B., Losch, M. & Lemieux, J.-F. Landfast sea ice material properties derived from ice bridge simulations using the maxwell elasto-brittle rheology. *The Cryosphere* **14**, 2137–2157 (2020).

[8] Liu, Y., Losch, M., Hutter, N. & Mu, L. A new parameterization of coastal drag to simulate landfast ice in deep marginal seas in the arctic. *Journal of Geophysical Research: Oceans* **127**, e2022JC018413 (2022).

[9] Divine, D. V., Korsnes, R., Makshtas, A. P., Godtliebsen, F. & Svendsen, H. Atmospheric-driven state transfer of shore-fast ice in the northeastern Kara Sea. *Journal of Geophysical Research C: Oceans* **110**, 1–13 (2005).

[10] Johnson, M. *et al.* Evaluation of Arctic sea ice thickness simulated by Arctic Ocean model intercomparison project models. *Journal of Geophysical Research: Oceans* **117** (2012).

[11] Fraser, A. *et al.* Antarctic landfast sea ice: A review of its physics, biogeochemistry and ecology. *Reviews of Geophysics* **61**, e2022RG000770 (2023).

[12] Cornish, S. *et al.* Rise and fall of sea ice production in the arctic ocean's ice factories. *Nature Communications* **13**, 7800 (2022).

[13] Labrousse, S. *et al.* Where to live? landfast sea ice shapes emperor penguin habitat around antarctica. *Science Advances* **9**, eadg8340 (2023).

[14] Cooley, S. W. *et al.* Coldest canadian arctic communities face greatest reductions in shorefast sea ice. *Nature Climate Change* **10**, 533–538 (2020).

[15] Laidler, G. J. *et al.* Travelling and hunting in a changing arctic: Assessing inuit vulnerability to sea ice change in igloolik, nunavut. *Climatic change* **94**, 363–397 (2009).

[16] Laidre, K. L. *et al.* Glacial ice supports a distinct and undocumented polar bear subpopulation persisting in late 21st-century sea-ice conditions. *Science* **376**, 1333–1338 (2022).

[17] Itkin, P., Losch, M. & Gerdes, R. Landfast ice affects the stability of the Arctic halocline: Evidence from a numerical model. *Journal of Geophysical Research: Oceans* **120**, 2622–2635 (2015).

[18] Sterlin, J. *et al.* Influence of the representation of landfast ice on the simulation of the Arctic sea ice and Arctic Ocean halocline. *Ocean Dynamics* **74**, 407–437 (2024).

[19] Martinson, D. G. & Iannuzzi, R. A. Spatial/temporal patterns in Weddell gyre characteristics and their relationship to global climate. *Journal of Geophysical Research: Oceans* **108** (2003).

[20] Beer, E., Eisenman, I., Wagner, T. J. & Fine, E. C. A possible hysteresis in the Arctic Ocean due to release of subsurface heat during sea ice retreat. *Journal of Physical Oceanography* **53**, 1323–1335 (2023).

[21] Polyakov, I. V., Pnyushkov, A. V. & Carmack, E. C. Stability of the Arctic halocline: a new indicator of Arctic climate change. *Environmental Research Letters* **13**, 125008 (2018).

[22] Polyakov, I. V. *et al.* Atlantification advances into the Amerasian Basin of the Arctic Ocean. *Science Advances* **11**, eadq7580 (2025).

[23] Polyakov, I. V. *et al.* Greater role for Atlantic inflows on sea-ice loss in the Eurasian Basin of the Arctic Ocean. *Science* **356**, 285–291 (2017).

[24] Martinson, D. G. & Steele, M. Future of the arctic sea ice cover: Implications of an antarctic analog. *Geophysical Research Letters* **28**, 307–310 (2001).

[25] Steele, M. & Boyd, T. Retreat of the cold halocline layer in the Arctic Ocean. *Journal of Geophysical Research: Oceans* **103**, 10419–10435 (1998).

[26] Newton, R., Schlosser, P., Martinson, D. G. & Maslowski, W. Freshwater distribution in the arctic ocean: simulation with a high-resolution model and model-data comparison. *Journal of Geophysical Research: Oceans* **113** (2008).

[27] Behrendt, A., Sumata, H., Rabe, B. & Schauer, U. A comprehensive, quality-controlled and up-to-date data set of temperature and salinity data for the Arctic Mediterranean Sea (Version 1.0) (2017).

[28] Behrendt, A., Sumata, H., Rabe, B. & Schauer, U. UDASH–Unified Database for Arctic and Subarctic Hydrography. *Earth System Science Data* **10**, 1119–1138 (2018).

[29] Paffrath, R., Laukert, G., Bauch, D., Rutgers van der Loeff, M. & Pahnke, K. Separating individual contributions of major Siberian rivers in the Transpolar Drift of the Arctic Ocean. *Scientific Reports* **11**, 1–11 (2021).

[30] Janout, M. A. *et al.* Kara Sea freshwater transport through Vilkitsky Strait: variability, forcing, and further pathways toward the western Arctic Ocean from a model and observations. *Journal of Geophysical Research: Oceans* **120**, 4925–4944 (2015).

[31] Asbjørnsen, H., Årthun, M., Skagseth, Ø. & Eldevik, T. Mechanisms underlying recent Arctic Atlantification. *Geophysical research letters* **47**, e2020GL088036 (2020).

[32] Ingvaldsen, R. B. *et al.* Physical manifestations and ecological implications of Arctic Atlantification. *Nature Reviews Earth & Environment* **2**, 874–889 (2021).

[33] Olason, E. A dynamical model of Kara Sea land-fast ice. *Journal of Geophysical Research: Oceans* **121**, 3141–3158 (2016).

[34] Duan, C., Dong, S., Xie, Z. & Wang, Z. Temporal variability and trends of sea ice in the Kara Sea and their relationship with atmospheric factors. *Polar Science* **20**, 136–147 (2019).

[35] Zatsepin, A. *et al.* On the mechanism of wind-induced transformation of a river runoff water lens in the Kara Sea. *Oceanology* **57**, 1–7 (2017).

[36] Zhang, J., Lindsay, R., Schweiger, A. & Steele, M. The impact of an intense summer cyclone on 2012 Arctic sea ice retreat. *Geophysical Research Letters* **40**, 720–726 (2013).

[37] Parkinson, C. L. & Comiso, J. C. On the 2012 record low Arctic sea ice cover: combined impact of preconditioning and an August storm. *Geophysical Research Letters* **40**, 1356–1361 (2013).

[38] Laukert, G. *et al.* Ocean circulation and freshwater pathways in the Arctic Mediterranean based on a combined Nd isotope, REE and oxygen isotope section across Fram Strait. *Geochimica et Cosmochimica Acta* **202**, 285–309 (2017).

[39] Peralta-Ferriz, C. & Woodgate, R. A. Seasonal and interannual variability of pan-Arctic surface mixed layer properties from 1979 to 2012 from hydrographic data, and the dominance of stratification for multiyear mixed layer depth shoaling. *Progress in Oceanography* **134**, 19–53 (2015).

[40] Janout, M. A. *et al.* On the variability of stratification in the freshwater-influenced Laptev Sea region. *Frontiers in Marine Science* **7**, 543489 (2020).

[41] Marshall, J., Adcroft, A., Hill, C., Perelman, L. & Heisey, C. A finite-volume, incompressible navier stokes model for studies of the ocean on parallel computers. *Journal of Geophysical Research: Oceans* **102**, 5753–5766 (1997).

[42] MITgcm Group. MITgcm User Manual. https://mitgcm.readthedocs.io/ (2022).

[43] Semtner, A. J. A model for the thermodynamic growth of sea ice in numerical investigations of climate. *Journal of Physical Oceanography* **6**, 379–389 (1976).

[44] Hibler, W. D. A dynamic thermodynamic sea ice model. *Journal of Physical Oceanography* **9**, 815–846 (1979).

[45] Zhang, J. & Hibler, W. D. On an efficient numerical method for modeling sea ice dynamics. *Journal of Geophysical Research: Oceans* **102**, 8691–8702 (1997).

[46] Dee, D. P. *et al.* The ERA-Interim reanalysis: configuration and performance of the data assimilation system. *Quarterly Journal of the Royal Meteorological Society* **137**, 553–597 (2011).

[47] Steele, M., Ermold, W. & Zhang, J. Modeling the formation and fate of the near-surface temperature maximum in the Canadian Basin of the Arctic Ocean. *Journal of Geophysical Research: Oceans* **116**, 1–13 (2011).

[48] Losch, M., Menemenlis, D., Campin, J. M., Heimbach, P. & Hill, C. On the formulation of sea-ice models. Part 1: Effects of different solver implementations and parameterizations. *Ocean Modelling* **33**, 129–144 (2010).

[49] Ungermann, M. & Losch, M. An observationally based evaluation of subgrid scale ice thickness distributions simulated in a large-scale sea ice-ocean model of the Arctic Ocean. *Journal of Geophysical Research: Oceans* **123**, 8052–8067 (2018).